Supplementary Information

The protease GtgE from Salmonella exclusively targets inactive Rab GTPases

Table of Contents

Supplementary Figures

Supplementary Figure 1

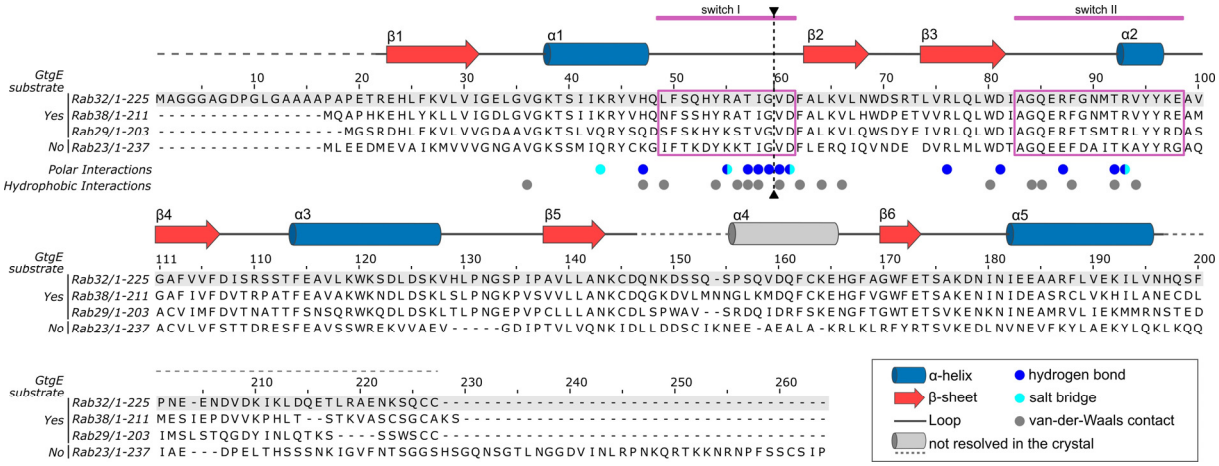

Supplementary Fig. 1. Sequence alignment of the GtgE-substrates Rab32, Rab38, and Rab29 in comparison to the non-GtgE substrate Rab23. Secondary structure annotations above the sequences refer to the Rab32:GDP:GtgE$_{C45A}$-complex. Blue or grey dots below the sequences indicate polar and hydrophobic interactions of Rab32 with GtgE in the complex structure. Magenta: switch regions; black arrow and dashed line: GtgE cleavage site in Rab32, Rab38, and Rab29.

Supplementary Figure 2

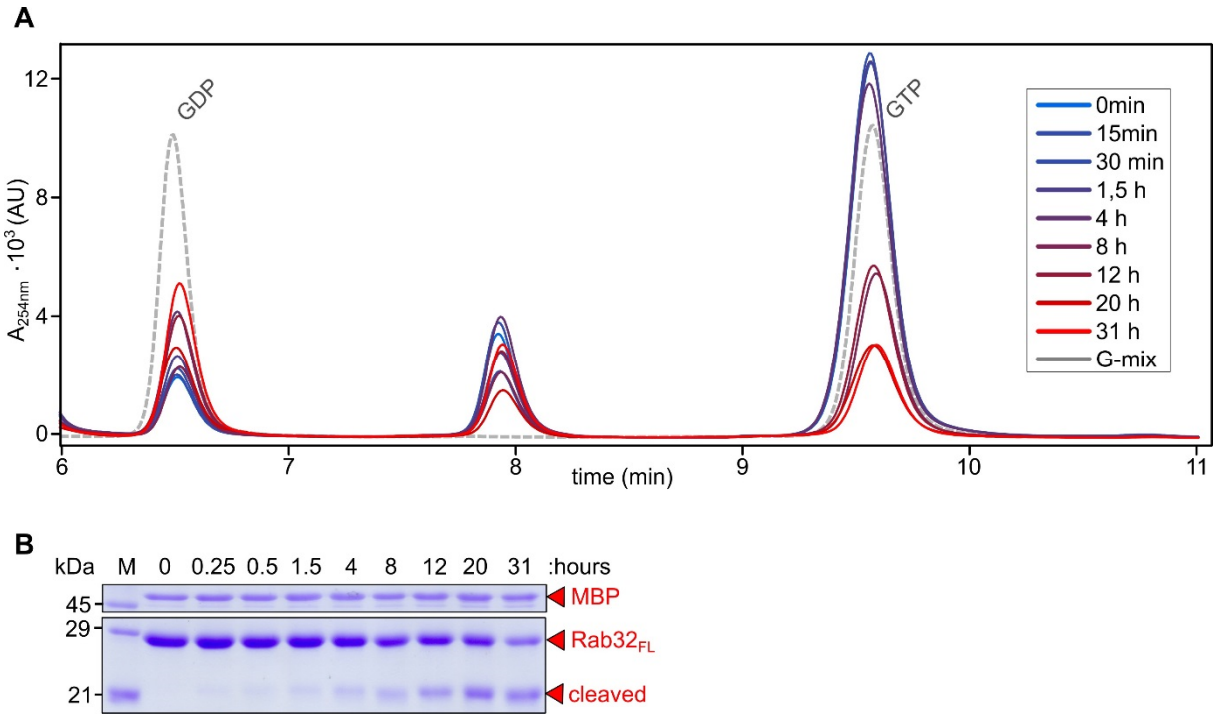

Supplementary Fig. 2. GTP-hydrolysis and proteolytic cleavage of Rab32:GTP.
(A) Intrinsic GTP-hydrolysis activity of Rab32. Time-dependent GTP-to-GDP-hydrolysis by Rab32 loaded with GTP was monitored using ion-pairing reversed phase chromatographic separation of GDP and GTP. Integrated peaks were used for the quantification of nucleotide content. The rate constant of GTP-hydrolysis was determined from single exponential fitting of the GTP-conversion with time (Fig. 1C). G-mix contains GDP and GTP as chromatographic references.
(**B**) Time-dependent GtgE-mediated (8 nM) cleavage of Rab32:GTP (8 µM final) in a SDS-PAGE based gel shift assay stained with Coomassie. MBP was used as internal standard for quantification. The observed rate constant for proteolysis was obtained from time-dependent single exponential fit of the $Rab32_{FL}$ concentration. The Rab32 level was determined from the SDS-PAGE band intensity, which was analyzed densitometrically (Fig. 1C).

Supplementary Figure 3

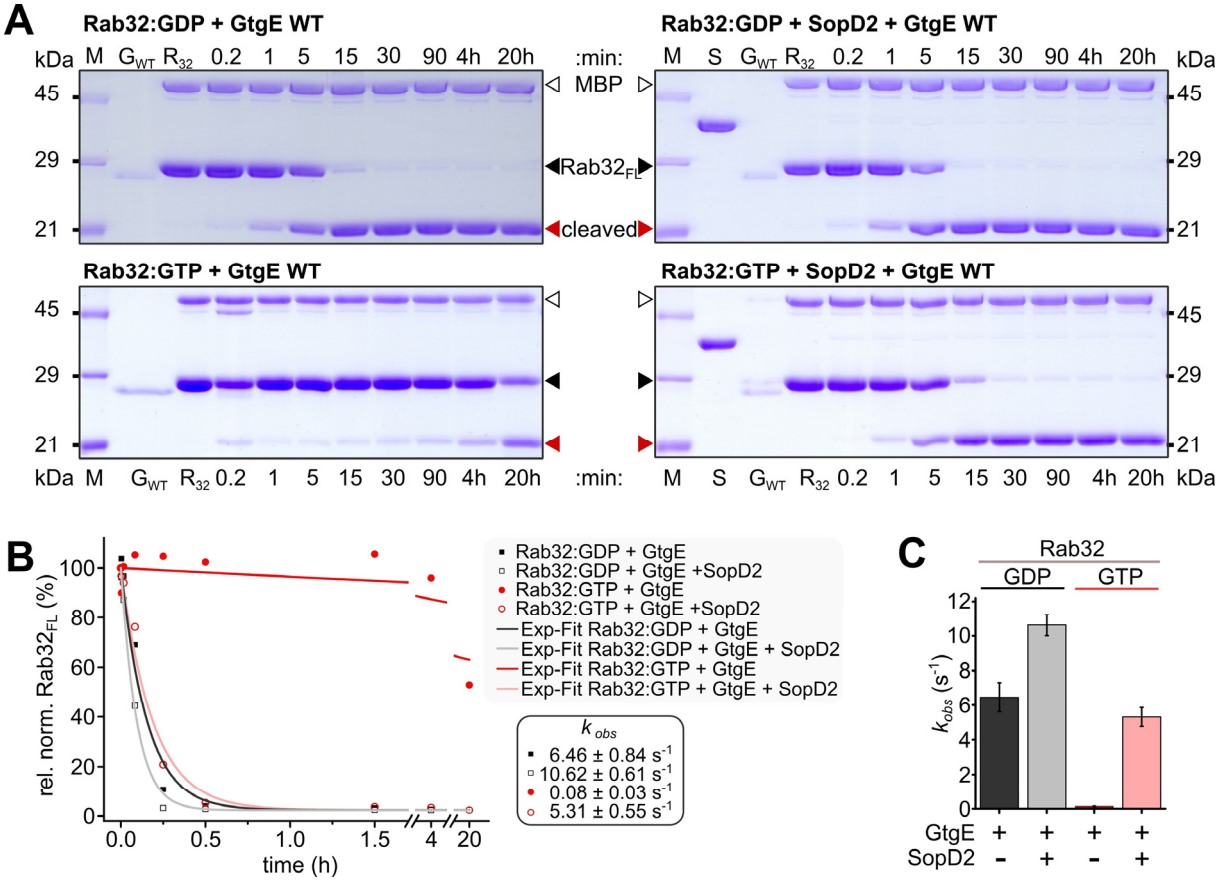

Supplementary Fig. 3. Dependence of Rab32-cleavage by GtgE on SopD2 mediated GTPase activation.

(**A**) SopD2 interference with GtgE mediated proteolytic Rab32 cleavage over time analysed by Coomassie-stained SDS-PAGE. $Rab32_{FL}$ (R_{32};8 µM) was challenged with GtgE (G_{WT}; 8 nM) and/or SopD2 (S; 80 nM). White triangle: MBP standard; black arrow $Rab32_{FL}$; red arrow cleavage product $Rab32_{60\text{-}225}$.

(**B**) Densitometric quantification of the time-dependent decrease of $Rab32_{FL}$ bands from A. Signal intensity was normalized for the internal standard MBP. Data was fitted to a single exponential function to yield the observed rate constants (k_{obs}) (bottom right).

(**C**) Bar graph of the determined rate constant from B.

Supplementary Figure 4

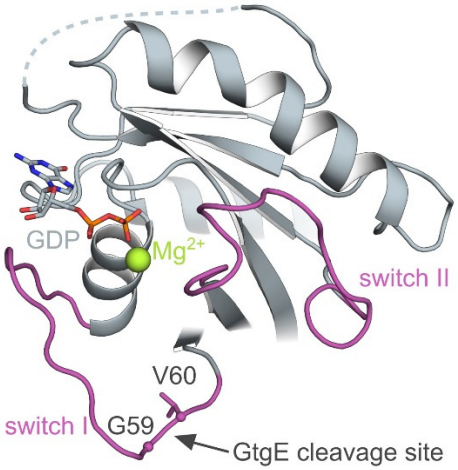

Supplementary Fig. 4. Structural context of the Rab32-cleavage site on the basis of the Rab32:GDP:GtgE$_{C45A}$-complex crystal structure. The GtgE cleavage site is highlighted in the ball and sticks representation of Rab32 residues Gly59 and Val60. Magenta loops: switch regions; sticks: GDP; green sphere: Mg^{2+}-ion.

Supplementary Figure 5

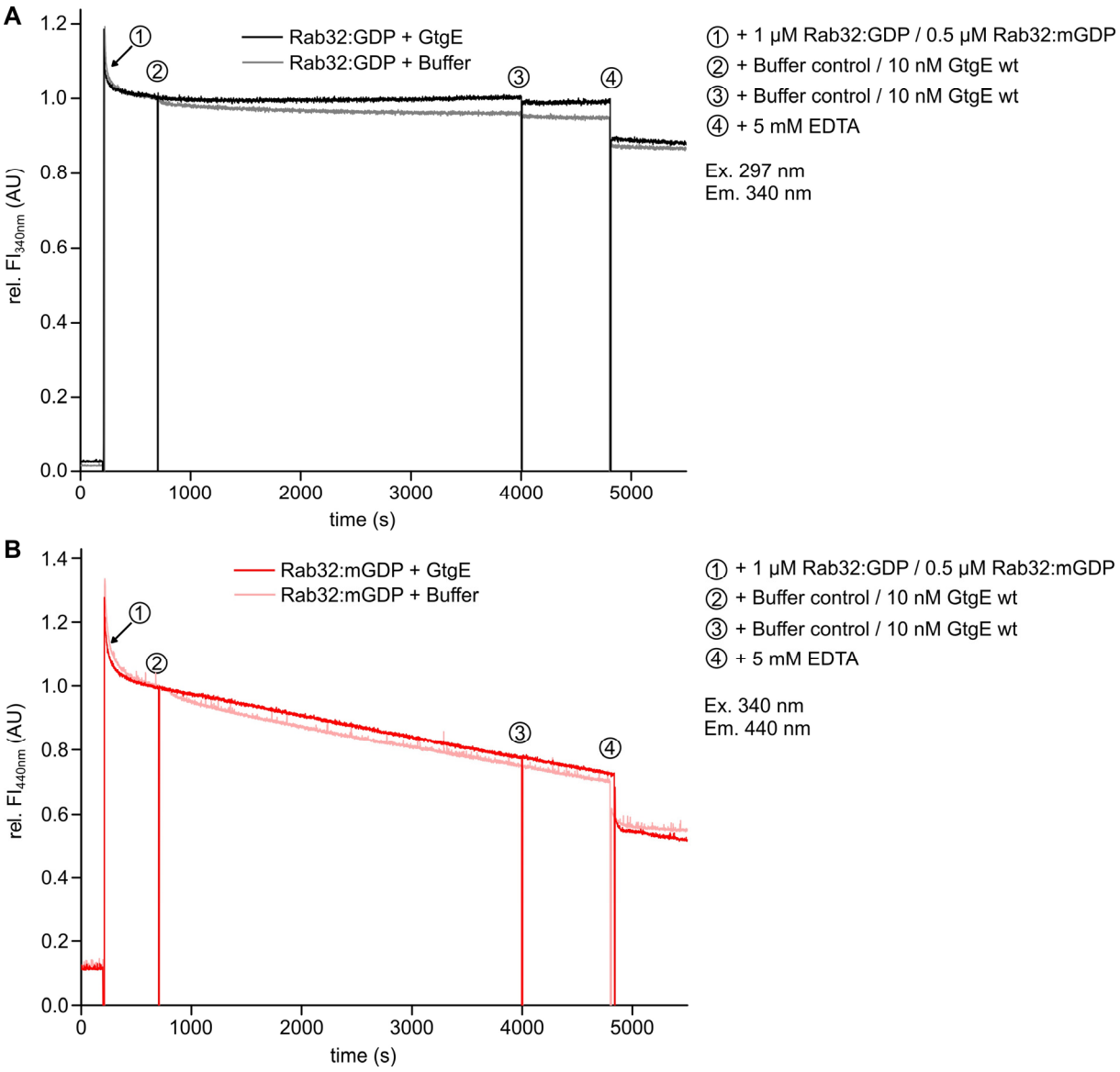

Supplementary Fig. 5. The GtgE-mediated Rab32-proteolysis cannot be monitored using established fluorescence methods. Rab32-proteolysis has been subjected to time dependent fluorescence experiments. Fluorescence intensity testing of GtgE-mediated Rab32-cleavage by Rab32 tryptophane fluorescence (**A**) or Rab32:mantGDP fluorescence (**B**). There is no significant difference of the fluorescence change in the absence or presence of GtgE, indicating that these assays are unsuitable for monitoring Rab32-proteolysis by GtgE.

Supplementary Figure 6

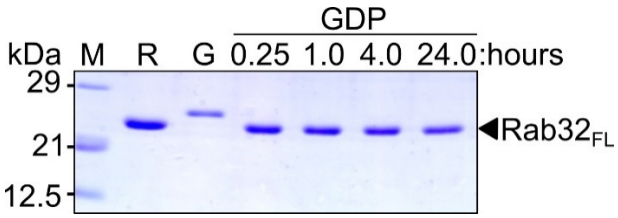

Supplementary Fig. 6. The GtgE-mutant $GtgE_{C45A}$ lacks proteolytic activity. $Rab32_{FL}$:GDP (R, 8 µM) was incubated with $GtgE_{C45A}$ (G, 8 nM) and samples were analyzed by Coomassie-stained SDS-PAGE at indicated time points. In contrast to wild type GtgE, the mutant $GtgE_{C45A}$ is proteolytically inactive as indicated by a lack of shift in $Rab32_{FL}$ molecular weight.

Supplementary Figure 7

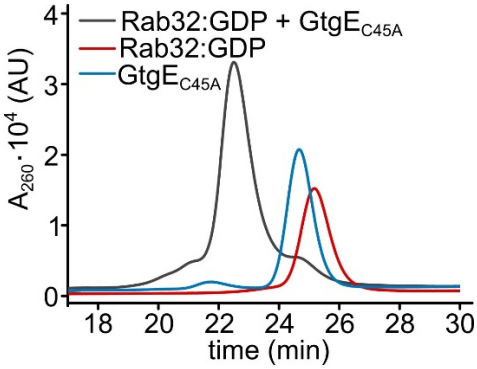

Supplementary Fig. 7. Complex formation of Rab32:GDP with $GtgE_{C45A}$ in analytical size exclusion chromatography. Rab32:GDP and $GtgE_{C45A}$ (8 µM each) were analyzed separately in SEC-buffer (supplemented with 10 µM GDP) as references. The decrease in elution time for the Rab32:GDP and $GtgE_{C45A}$ complex mixture indicates an increase in molecular weight relative to the individual proteins and demonstrates successful complex formation.

Supplementary Figure 8

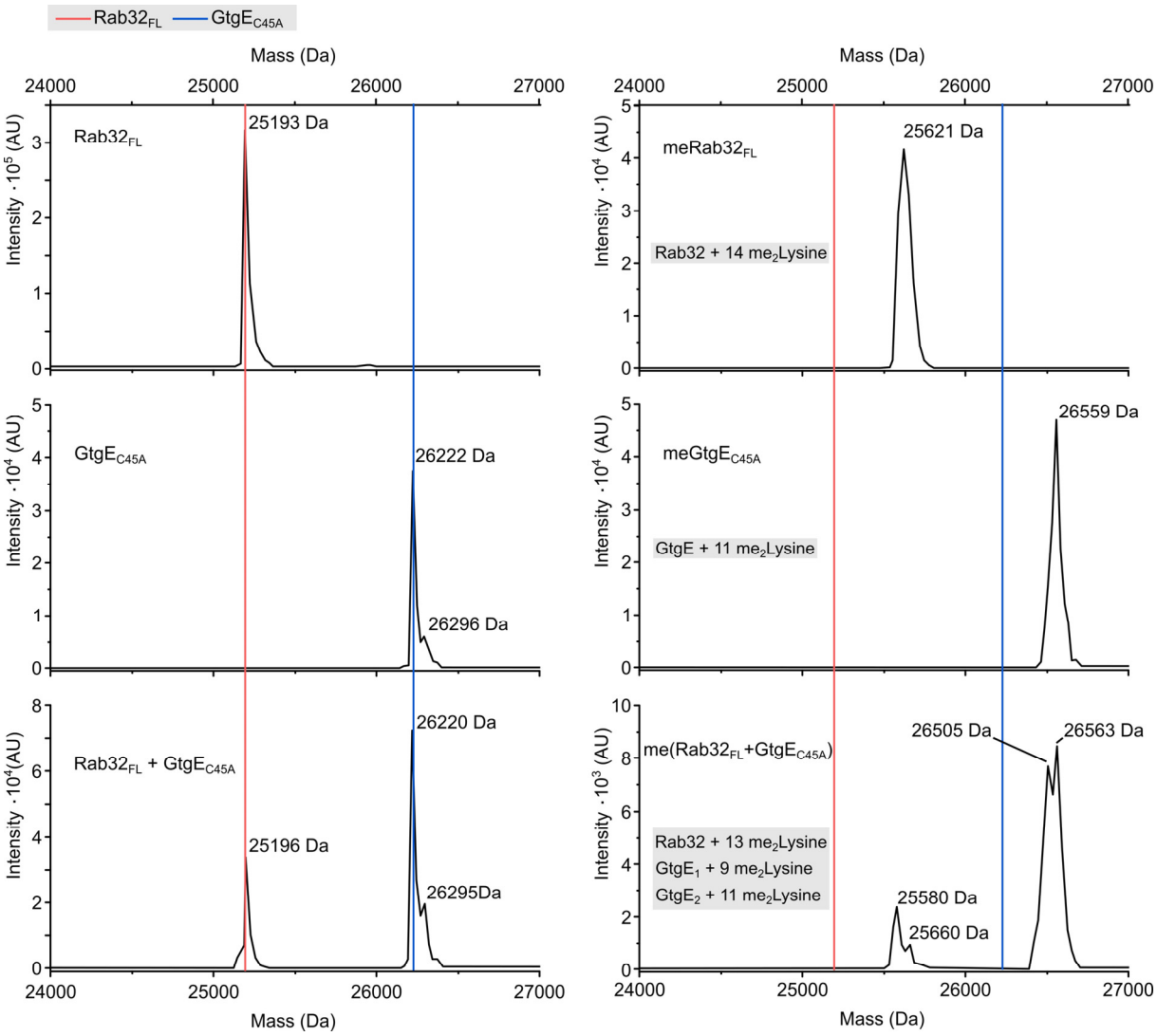

Supplementary Fig. 8. Mass spectrometry analysis of the methylated full length Rab32:GDP:GtgE$_{C45A}$ complex.

Left panel: top, Rab32$_{FL}$; middle, GtgE$_{C45A}$; bottom, 1:1 mixture of Rab32$_{FL}$ and GtgE$_{C45A}$.

Right panel: analysis of methylated (me) proteins (top, meRab32$_{FL}$; middle, meGtgE$_{C45A}$; bottom, 1:1 mixture of the preformed complex me(Rab32$_{FL}$:GtgE$_{C45A}$)). The red and blue lines indicate the theoretical masses of Rab32$_{FL}$ ($M_{cal(Rab32,FL)}$ = 25191 Da) and GtgE$_{C45A}$ ($M_{cal(GtgE,C45A)}$ = 26226 Da), respectively. Grey boxes: number of detected dimethylated lysines in the corresponding experiments.

Supplementary Figure 9

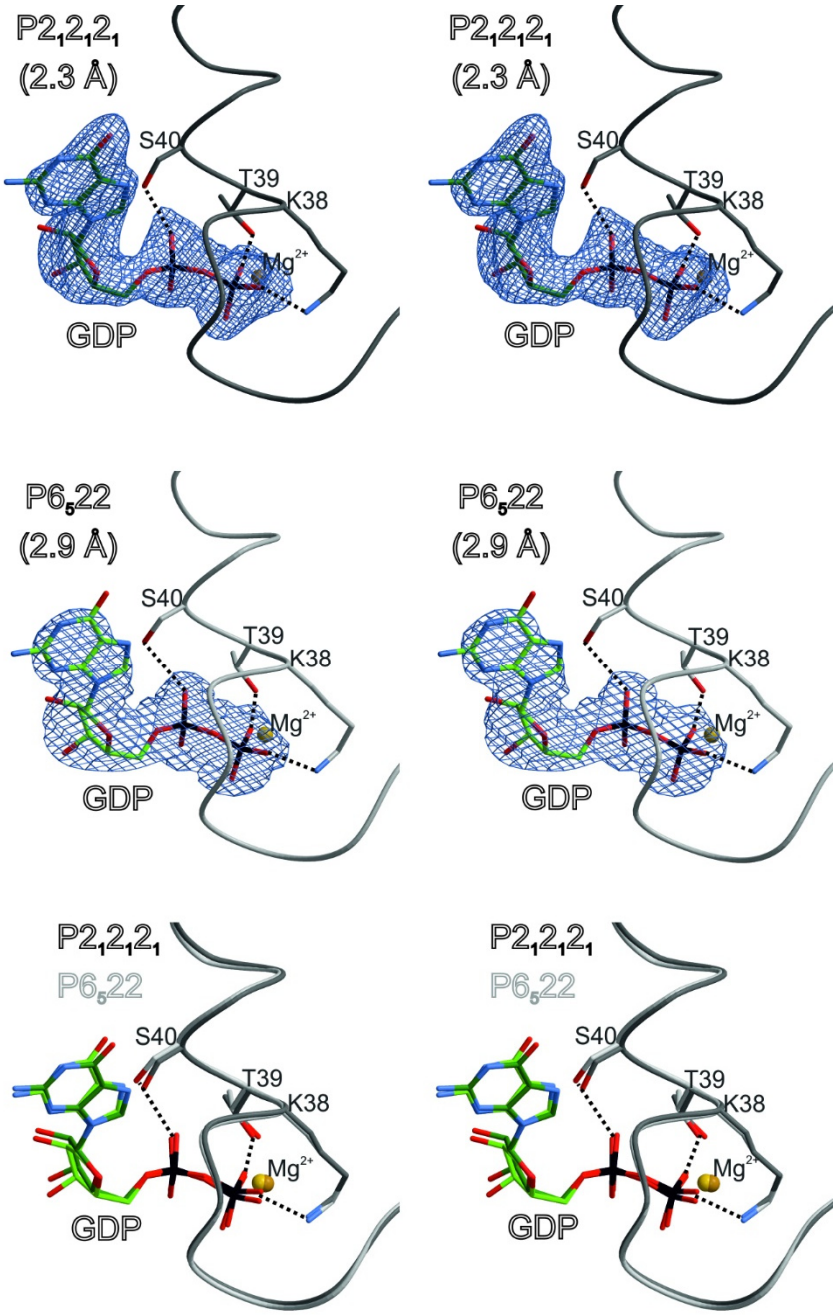

Supplementary Fig. 9. Comparison of the electron density of GDP in the full length and truncated Rab32:GtgE$_{C45A}$ complex structures depicted as stereo-view images.
Sections of the P-loop, the GDP-molecule and the magnesium ion of Rab32$_{18-201}$:GDP:GtgE$_{21-214,C45A}$ (top panel, PDB ID: 5OEC, space group $P2_12_12_1$, 2.3 Å resolution) and Rab32$_{FL}$:GDP:GtgE$_{FL,C45A}$ (middle panel, PDB ID: 5OED, space group $P6_522$, 2.9 Å resolution), respectively. The $2F_O–F_C$ electron-density maps depict the GDP nucleotides, which have been excluded prior to phase calculations (blue mesh, contour level at 1σ).
Structural superposition of both crystal structures revealing a close match of both complexes within this region (bottom panel).

Supplementary Figure 10

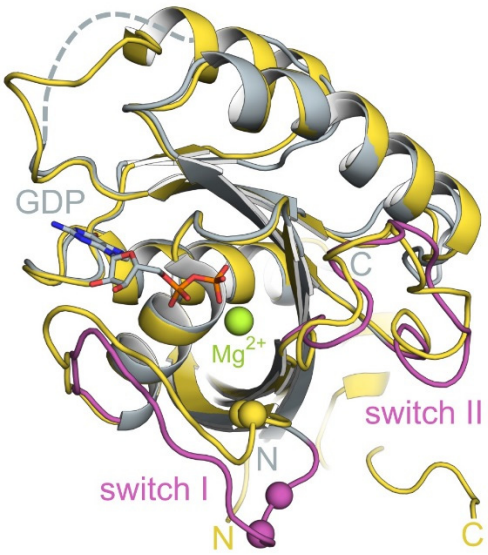

Supplementary Fig. 10. Structural superposition of Rab32 from the Rab32:GDP:$GtgE_{C45A}$ complex (grey) and Ypt1 from the yeast Ypt1:GDP:GDI complex (yellow, PDB ID: 1UKV [1]). The switch regions (indicated as magenta loops in Rab32) adopt a similar conformation that is clearly different from the active, GTP-bound conformations (see Fig. 3B). The switch structures are more reminiscent of but not equal to a GDI-bound state. Spheres: Cα-atoms of the GtgE cleavage site with the homologue positions also indicated in Ypt1; sticks: GDP; green sphere: Mg^{2+}-ion.

Supplementary Figure 11

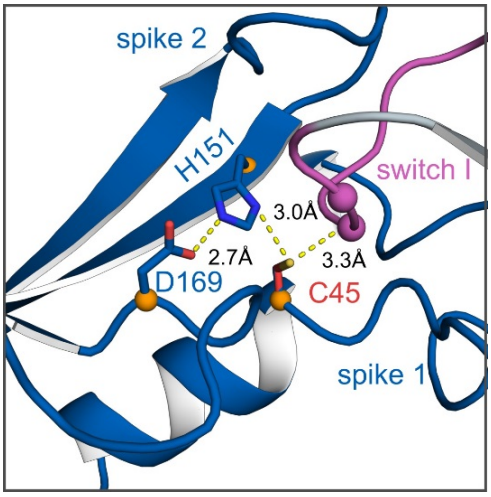

Supplementary Fig. 11. Model of the active catalytic triade in GtgE with the Rab32-substrate bound to the active site. The inactivating GtgE-mutation $C45A_G$ was reversed *in silico* using the PyMOL software [2], revealing a correctly aligned cysteine protease catalytic triad (*i.e.* constituted by $C45_G$, $H151_G$, and $D169_G$). Magenta loop: switch I of Rab32 from the Rab32:GDP:GtgE-complex; orange spheres and sticks: Cα-atoms and residues forming the catalytic triad, respectively; red sticks: *in silico* positioned cysteine at position 45 of GtgE in exchange for alanine; yellow dashed lines: distance measurements.

Supplementary Figure 12

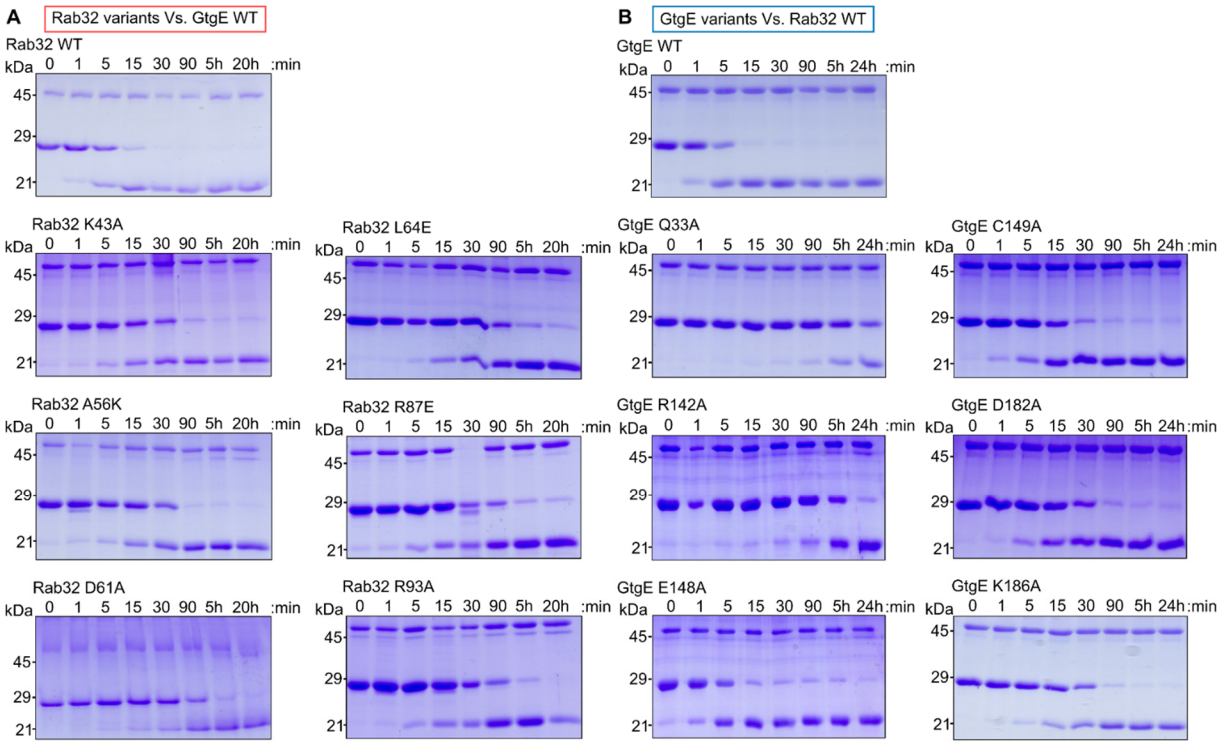

Supplementary Fig. 12. Mutational analysis of Rab32 and GtgE using a Coomassie-stained SDS-PAGE-based proteolytic Rab32 cleavage assay. These data form the basis for determining proteolytic rate constants as described in Supplementary Fig. 13.
(**A**) Proteolysis of Rab32:GDP and mutants thereof (8 µM) by wild type GtgE (8 nM).
(**B**) Proteolysis of Rab32:GDP (8 µM) with GtgE and mutants thereof (8 nM).

Supplementary Figure 13

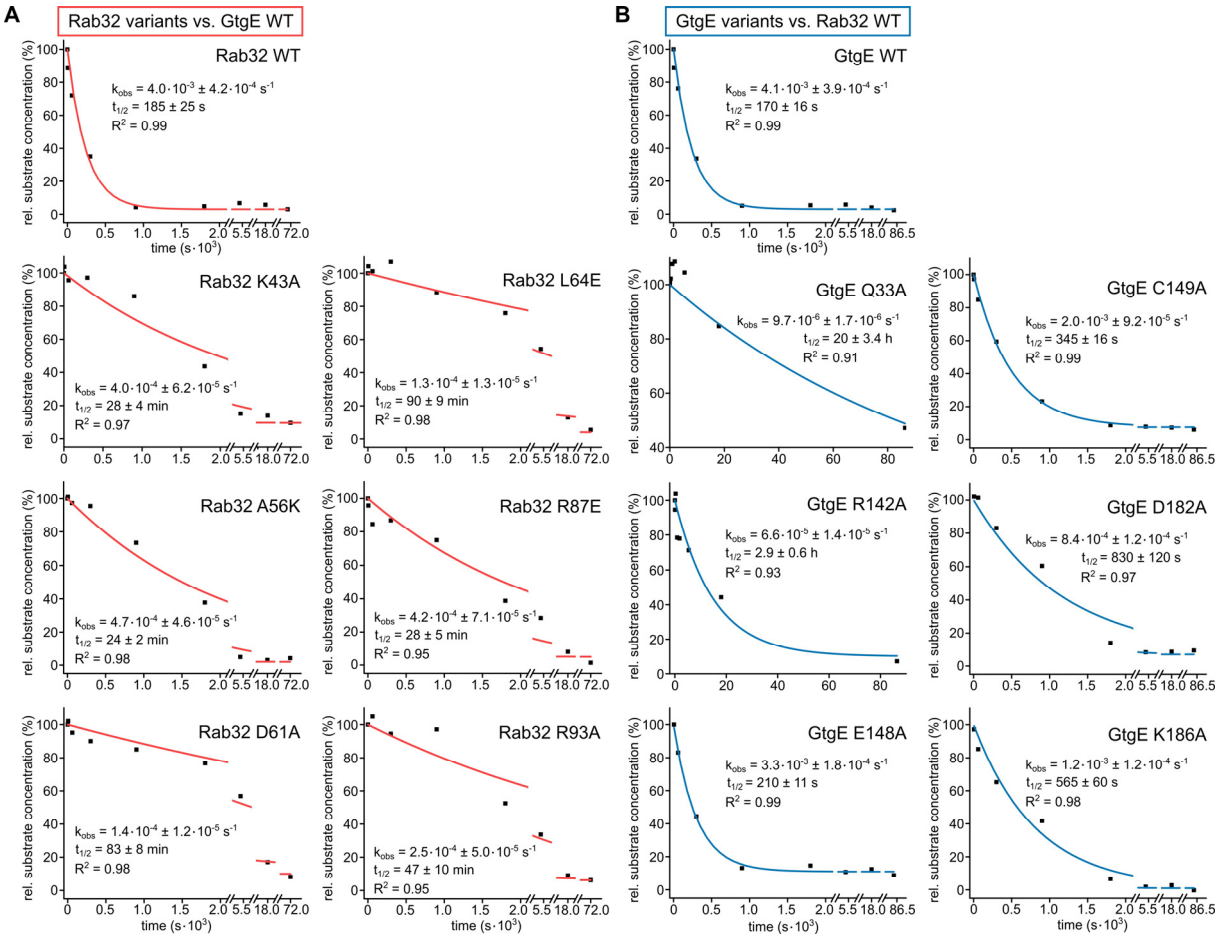

Supplementary Fig. 13. Determination of proteolytic rates GtgE for the Rab32-substrate and mutants thereof. Results are based on densitometric analysis of proteolytic Rab32-cleavage assays monitored by Coomassie-stained SDS-PAGE (Supplementary Fig. 12). The time-dependent decrease of $Rab32_{FL}$ was fitted to a single exponential function to yield the observed rate constants (k_{obs}). The k_{obs}-values have also been converted to half-lives ($t_{1/2}$) following the relationship $t_{1/2}$ = ln 2 / k_{obs}. Single exponential fits correspond to the experimental data very well as indicated by an R^2-value close to 1. Errors represent the standard deviation of the exponential fit.

(**A**) Rab32:GDP mutants (8 µM) and wild type incubated with wild type GtgE (8 nM) (red curves).

(**B**) GtgE mutants and wild type (both 8 nM final) were incubated with wild type Rab32:GDP (8 µM) (blue curves).

Supplementary Figure 14

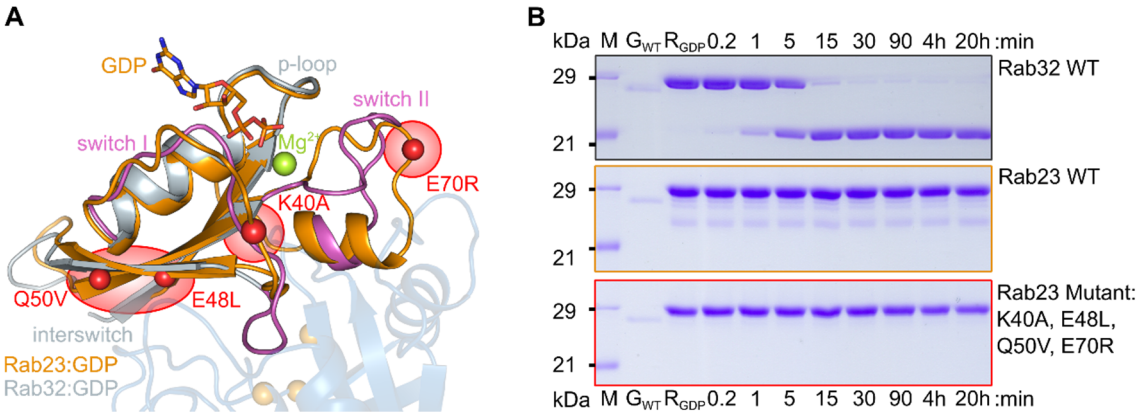

Supplementary Fig. 14. Exploration of the GtgE Rab-substrate specificity with a selected Rab23 mutant. Choice of mutation positions was guided by sequence alignment and interaction site analysis from the Rab32:GtgE-complex (see Supplementary Fig. 1).
(**A**) Structural superposition of the Rab23:GDP (orange) and Rab32:GDP (grey) in complex with $GtgE_{C45A}$ (blue, transparent) depicted as cartoon. Mutations in Rab23 to the corresponding amino acid from Rab32 were identified in three hot spots highlighted in red circles: switch I (K40A); interswitch (E48L; Q50V); switch II (E70R). Highlighted as red spheres: C_α-atoms of respective mutations, sticks: GDP, magenta: switch regions, green sphere: Mg^{2+}-ion.
(**B**) Time dependent GtgE proteolysis gel shift assay of Rab32:GDP, Rab23:GDP, and Rab23:GDP mutant (K40A; E48L; Q50V; E70R). GtgE is unable to cleave Rab23 or Rab23-mutant containing respective Rab32-mutations, indicating that further structural determinants contribute to the Rab-specificity of the protease. Abbreviations: GtgE WT (G_{WT}, 8 nM), respective GDP-bound Rab (R_{GDP}, all 8 µM) without GtgE added.

Supplementary Figure 15

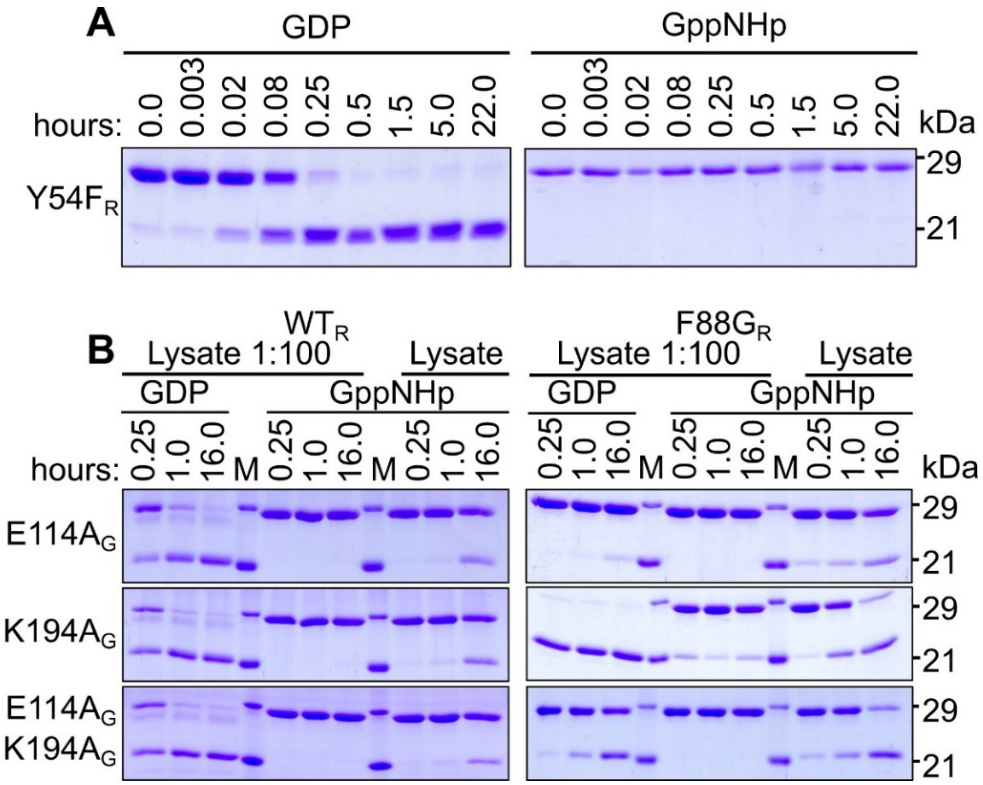

Supplementary Fig. 15. Qualitative analysis of the impact of mutations in potential nucleotide specificity hubs by gel shift activity assay.

(**A**) Significance of hub 2 mutant Y54F$_R$ loaded with GDP or GppNHp (compare with Fig. 5D).

(**B**) Significance of hub 3 mutants: Rab F88G loaded with GDP or GppNHp was treated with cleared *E. coli* lysate (or 1:100 diluted lysate) with overexpressed GtgE E114A, K194A, or the double mutant over time, respectively (see Fig. 5F).

Supplementary Figure 16

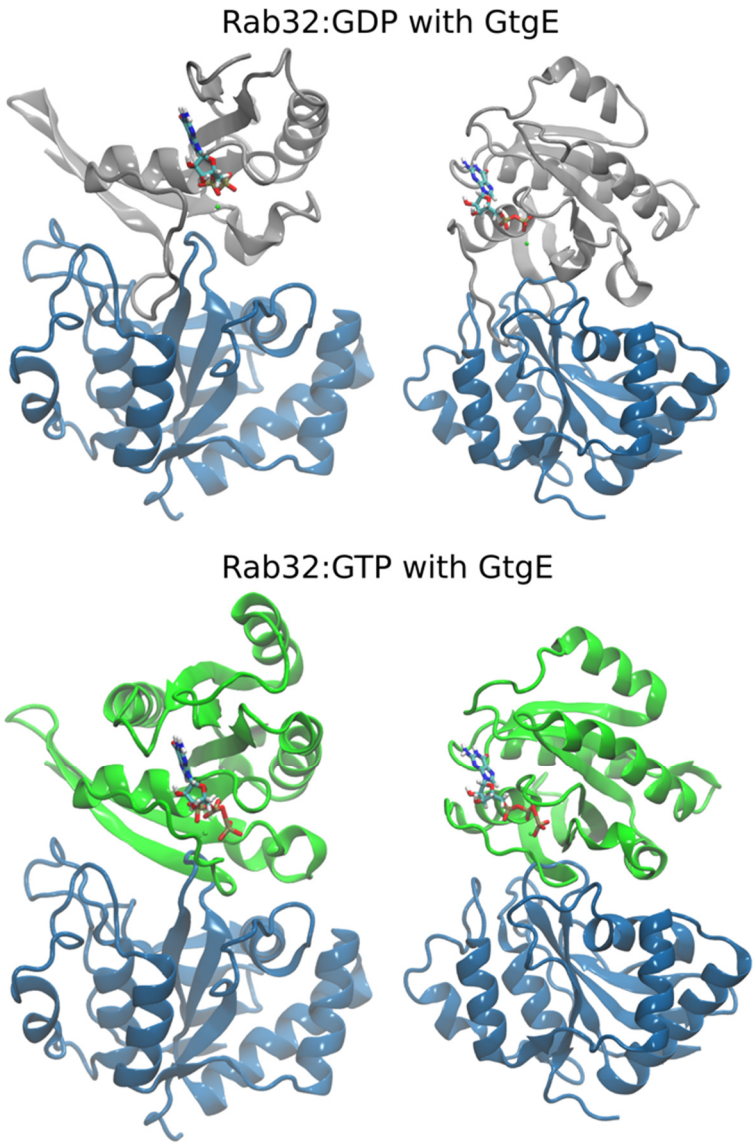

Supplementary Fig. 16. Models of GDP-bound (top panel) and a hypothetical GTP-bound Rab32 (bottom panel) in complex with wild type GtgE as starting points for atomistic molecular dynamics simulations. The GDP-bound Rab:GtgE complex is constituted based on the presented crystal structure from this work. The hypothetical GTP-bound complex structure is based on the active state Rab32 in complex with $GppCH_2p$ and its effector binding domain VARP-ANKRD1 (PDB ID: 4CYM). Only the hypothetic Rab32:GTP:GtgE results in steric conflicts along the protein-protein interface particularly in the Rab switch I region with the spike 2 loop in GtgE. Both complexes are additionally shown 45° tilted on the y-axis.

Supplementary Figure 17

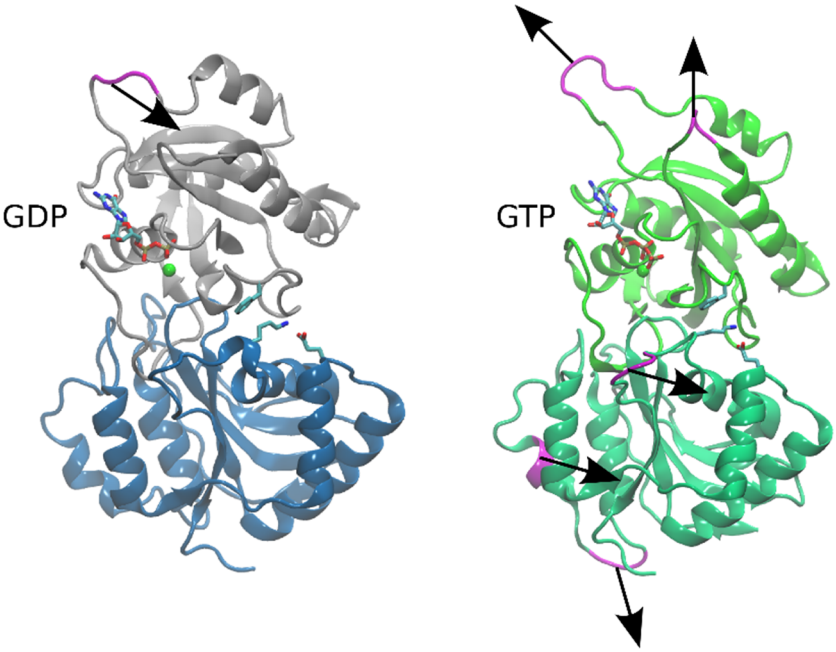

Supplementary Fig. 17. Principal component analysis of the Rab32:GtgE-complex in two different activity states. The figure shows the first modes of the principal component analysis of the Rab32:GDP:GtgE-complex (left) and the putative Rab32:GTP:GtgE-complex (right). While Rab32 (grey) of the GDP-complex only shows a single movement of a loop structure (purple), the GTP-complex reveals movements of two loop structures in Rab32 (light green) and three movements in GtgE (dark green). Interestingly, most of the movements of the GTP-complex point away from the interaction site of Rab32 and GtgE, while the movement of the GDP-complex points towards the interaction site of both domains. The diametral protein movements in the GTP-complex are supporting the complex dissociation for active Rab32:GTP, consistent with the strict GDP-state preference of GtgE for Rab32. The normal modes shown here, indicated by black arrows, comprise *ca*. 74% (GDP-complex) and *ca*. 77 % (GTP-complex) of their overall global motion.

Supplementary Figure 18

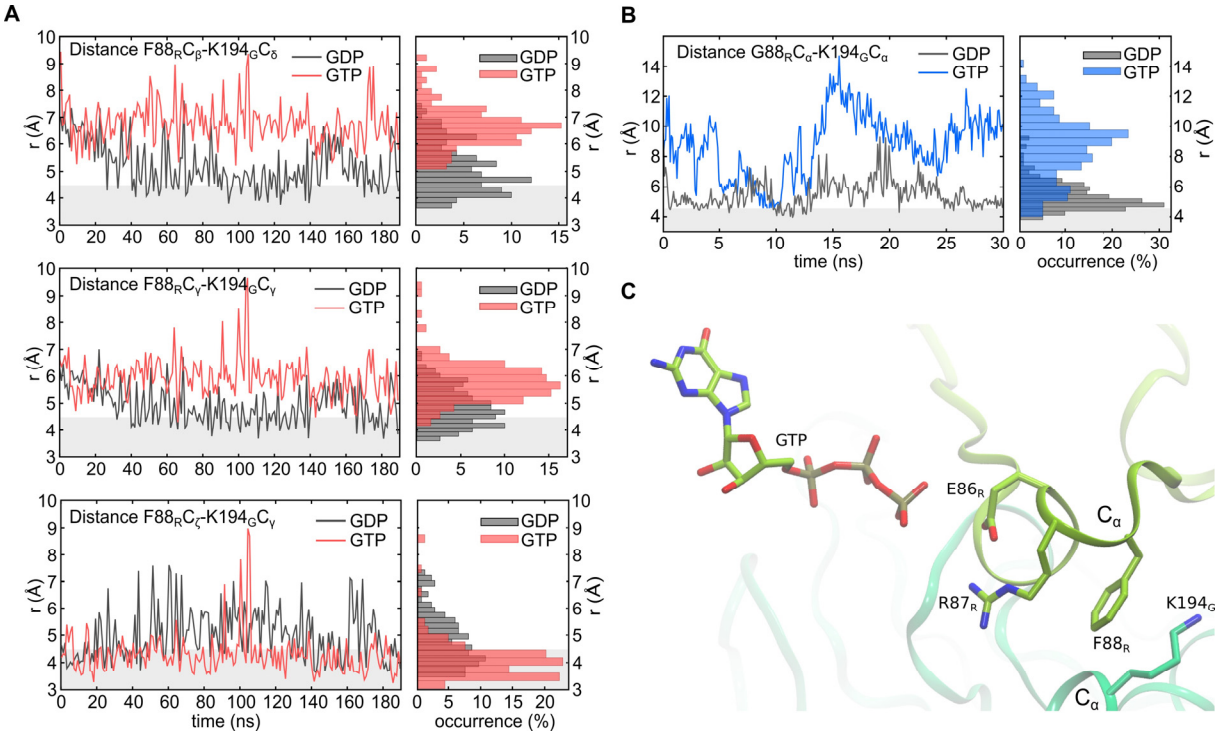

Supplementary Fig. 18. Selected atom pair distances in a GDP-bound and hypothetical GTP-bound Rab32:GtgE-complex from MD-simulations (left panels), and respective distance occurrences shown as histograms (right panels). The distance threshold for van-der-Waals interactions (<4.5 Å) is marked as grey shaded area.

(**A**) The $F88_R$ may form a decisive element for the GDP-state preference of GtgE toward Rab32. Specific atom-pair distances are shown for $F88_R$ of Rab32 and $K194_G$ GtgE (*top panel*: $F88_RC_\beta$-$K194_GC_\delta$, *middle*: $F88_RC_\gamma$-$K194_GC_\gamma$, *bottom*: $F88_RC_\zeta$-$K194_GC_\gamma$) from MD-simulations of the GDP- (in black) and GTP-bound (in red) Rab32:GtgE-complexes (see Fig. 5B right panels). A hydrophobic interaction between $F88_R$ and $K194_G$ is indicated based on all traces in the GDP-bound complex (black), whereas the hypothetic GTP-bound complex leads to an increase in the distance between $F88_RC_\beta$-$K194_GC_\delta$ and $F88_RC_\gamma$-$K194_GC_\gamma$, but not between $F88_RC_\zeta$-$K194_GC_\gamma$ (in red). This suggests that the van-der-Waals interactions between Rab32 and GtgE are decreased in the hypothetical GTP-state, which could lead to dissociation of GtgE from Rab32.

(**B**) Atom-pair distances in the $F88G_R$ mutant based on MD simulations of the GDP- (in black) and GTP-bound (in red) Rab32:GtgE-complexes. In $F88G_R$, a higher population of $G88_R$-$K194_G$ interactions (<4.5 Å) are formed relative to the wild type (Fig. 5E).

(**C**) Structural representation of the MD simulation of the hypothetical GTP-bound Rab32:GtgE-complex after 190 ns. Highlighted in sticks: hub 1 residue $E86_R$ with $R87_R$ forming an ion pair (see Fig. 5A and Fig. 5F, top) and the hub 3 resides $F88_R$ and $K194_G$ with an distance increase of the C_α-atoms (see Fig. 5E, bottom).

Supplementary Tables

Supplementary Table 1.
Crystallographic statistics of the full length and truncated Rab32:GDP:GtgE$_{C45A}$-complex.

		Rab32 (18-201):GDP-GtgE (21-214) C45A	**Rab32:GDP-GtgE C45A**
Crystal parameters			
Space group		$P2_12_12_1$	$P6_522$
Cell constants (Å)		a = 47.8 , b = 67.0	a = b = 67.4
		c = 111.1	c = 427.3
Copies in asym. unit		1	1
Data collection & processing			
X-ray source		SLS, X06DA	SLS, X06DA
Wavelength (Å)		1.0	1.0
Resolution range (Å)[a]		50-2.3 (2.4-2.3)	50-2.9 (3.0-2.9)
No. observations		82247	69825
No. unique observations		16142	13564
Completeness (%)[a]		97.4 (93.0)	96.8 (98.1)
R_{merge} (%)[a,b]		8.2 (52.3)	6.2 (53.2)
$CC_{1/2}$ (%)[a]		99.7 (89.6)	99.9 (83.4)
I/σ (I)[a]		13.8 (3.6)	18.9 (2.9)
Refinement			
Resolution range (Å)		15-2.3	15-2.9
No. refl. working set		16068	13425
No. refl. test set		1603	1343
No. non hydrogen (protein)		2838	2906
No. of ligand atoms	GDP	28	28
	Mg	1	1
Water molecules		55	13
R_{work}/R_{free} (%)[c]		20.8 / 24.5	20.1 / 24.0
r.m.s.d. bond (Å) / (°)[d]		0.002 / 0.435	0.004 / 0.527
Average B-factor (Å^2)	Protein	56.6	85.2
	GDP; Mg	60.2	114.5
	Water	42.7	57.1
Ramachandran Plot (%)[e]		97.3 / 2.4 / 0.3	97.7 / 2.0 / 0.3

[a] The values in parentheses of resolution range, completeness, R_{merge}, $CC_{1/2}$ and I/σ (I) correspond to the last resolution shell. [b] $R_{merge}(I) = \sum_{hkl}\sum_j |[I(hkl)_j - I(hkl)]|/ \sum_{hkl} I_{hkl}$, where $I(hkl)_j$ is the measurement of the intensity of reflection *hkl* and $\langle I(hkl)\rangle$ is the average intensity. [c] $R = \sum_{hkl} | |F_{obs}| - |F_{calc}| |/\sum_{hkl} |F_{obs}|$, where R_{free} is calculated without a sigma cut off for a randomly chosen 5% of reflections, which were not used for structure refinement, and R_{work} is calculated for the remaining reflections. [d] Deviations from ideal bond lengths/angles. [e] Number of residues in favored region / allowed region / outlier region.

Supplementary Table 2.
Molecular interactions in the Rab32:GDP:GtgE-complex between $Rab32_{18-201}$:GDP and $GtgE_{21-214,\ C45A}$ (Fig. 3E). (**A**) Polar interactions including salt bridges with the respective atom distances of interacting atom pairs. (**B**) Hydrophobic interactions shown as in A.

A

Polar Interactions		
Rab32	**Distance (Å)**	**$GtgE_{C45A}$**
G59 (O)	**2.44**	Q33 (NE2)
V60 (O)	**2.62**	S144 (OG)
T57 (O)	**2.67**	L150 (N)
D61 (O)	**2.70**	G146 (N)
D81 (N)	**2.75**	G146 (O)
D61 (OD1)	**2.76**	L145 (N)
T57 (OG1)	**2.88**	G80 (N)
R76 (NE)	**2.89**	N39 (OD1)
D61 (OD2)	**2.92**	R142 (NH2)
R76 (NH2)	**2.93**	T37 (O)
H47 (NE2)	**3.03**	I77 (O)
D61 (OD1)	**3.10**	R142 (NH1)
R55 (NH2)	**3.14**	E79 (OE2)
I58 (N)	**3.14**	I81 (O)
R55 (NH1)	**3.22**	D82 (OD2)
R93 (NE)	**3.23**	D182 (OD1)
G59 (N)	**3.24**	L150 (O)
R93 (NH2)	**3.27**	D182 (OD1)
I58 (O)	**3.29**	I81 (N)
G59 (O)	**3.36**	A45 (N)
V60 (O)	**3.41**	C149 (SG)
R87 (NH1)	**3.42**	K194 (O)
R93 (NH2)	**3.51**	S179 (OG)
D61 (O)	**3.52**	S147 (N)
D81 (O)	**3.68**	S147 (N)
V60 (N)	**3.70**	N43 (OD1)
D61 (O)	**3.80**	L145 (N)
Salt Bridges		
Rab32	**Distance (Å)**	**$GtgE_{C45A}$**
K43 (NZ)	**4.00**	E148 (OE1)
K43 (NZ)	**3.69**	E148 (OE2)
R55 (NE)	**3.34**	E79 (OE2)
R55 (NH1)	**3.22**	D82 (OD2)
R55 (NH2)	**3.14**	E79 (OE2)
R93 (NE)	**3.23**	D182 (OD1)
R93 (NE)	**3.92**	D182 (OD2)
R93 (NH2)	**3.27**	D182 (OD1)
R93 (NH2)	**3.97**	D182 (OD2)
D61 (OD1)	**3.55**	R142 (NH2)
D61 (OD1)	**3.10**	R142 (NH1)
D61 (OD2)	**2.92**	R142 (NH2)
D61 (OD2)	**3.86**	R142 (NH1)

B

Hydrophobic Interactions		
Rab32	**Distance (Å)**	**$GtgE_{C45A}$**
L64	**3.5**	F34
F62	**3.5**	M171
V94	**3.7**	L145
V60	**3.8**	L41
W80	**3.8**	L145
L64	**3.9**	L41
I58	**3.9**	W46
H47	**3.9**	L78
I58	**3.9**	I81
T92	**3.9**	D185
I58	**3.9**	I202
I58	**4.0**	C86
L49	**4.1**	L78
A56	**4.1**	I83
I58	**4.1**	I141
V94	**4.1**	D185
G59*	**4.2***	A45*
I58	**4.2**	L150
I58	**4.2**	A152
F88	**4.2**	K194
Q85	**4.2**	Y195
V66	**4.3**	N39
T57	**4.3**	N76
V60	**4.3**	M171
T36	**4.4**	E148
Y54	**4.4**	E148
G84	**4.4**	Y195
[V60	4.5	N43
T36	4.5	E148
A56	4.5	C149
D61	4.5	H151
V94	4.5	K186
F88	4.5	Y195]

* Interaction not shown in Fig. 3E due to mutation in GtgE C45A

[ ] potential Interactions with a distance of 4.5 Å not shown in Fig. 3E (bottom)

Supplementary Table 3.

Kinetic parameters of GtgE-activity for Rab32:GDP. Data are calculated from conversion rates of $Rab32_{FL}$ bands in a densitometric analysis from Coomassie-stained SDS-PAGE assays (Supplementary Fig. 12, 13).

GtgE	Rab32	k_{cat}/K_M ($s^{-1}M^{-1}$)	Activity relative to WT (%)
WT	WT	$5.1 \times 10^5 \pm 4.9 \times 10^4$	100.0
Q33A	WT	$1.2 \times 10^3 \pm 2.1 \times 10^2$	0.2
R142A	WT	$8.3 \times 10^3 \pm 1.8 \times 10^3$	1.6
E148A	WT	$4.2 \times 10^5 \pm 2.2 \times 10^4$	82.0
C149A	WT	$2.5 \times 10^5 \pm 1.2 \times 10^4$	49.3
D182A	WT	$1.0 \times 10^5 \pm 1.5 \times 10^4$	20.5
K186A	WT	$1.5 \times 10^5 \pm 1.5 \times 10^4$	30.0
WT	K43A	$5.1 \times 10^4 \pm 7.8 \times 10^3$	10.0
WT	A56K	$6.1 \times 10^4 \pm 6.8 \times 10^3$	12.0
WT	D61A	$1.7 \times 10^4 \pm 1.6 \times 10^3$	3.4
WT	L64E	$1.6 \times 10^4 \pm 1.7 \times 10^3$	3.2
WT	R87E	$3.1 \times 10^4 \pm 6.2 \times 10^3$	6.0
WT	R93A	$5.2 \times 10^4 \pm 8.9 \times 10^3$	10.2

Supplementary References

1. Rak A*, et al.* Structure of Rab GDP-dissociation inhibitor in complex with prenylated Ypt1 GTPase. *Science* **302**, 646-650 (2003).

2. Schrodinger L. The PyMOL Molecular Graphics System, Version 1.8. (2015).